Int. J. Rock Mech. Min. Sci. & Geomech. Abstr. Vol. 23, No. 3, pp. 233–243, 1986
Printed in Great Britain

0148-9062/86 $3.00 + 0.00
Pergamon Journals Ltd

# Characterization of Rock Fissure Hydraulic Conductivity Using Idealized Wall Roughness Profiles

D. ELSWORTH*
R. E. GOODMAN†

*Changes in fissure hydraulic conductivity that accompany shear and normal rock joint displacements may have a profound effect on total discharges into engineered rock structures. The aperture changes that result from post-peak shear strength deformations commonly overshadow those corresponding to the pre-peak displacements. The form of the post-peak displacements are tensional and shear-dilational opening of fissures. If the surfaces of the matched fissures are idealized as either a sinusoidal or sawtooth form, the changes in hydraulic conductivity that accompany these displacement modes may be evaluated analytically. Assumptions inherent within this characterization approach relate to whether the flow may be considered as non-tortuous or tortuous. The former case allows exact analytical expressions to be developed for the conductivity; the latter requires certain simplifying assumptions to be made. For tortuous flow, the approximate analytical representation of the hydraulic conductivity is compared with a numerical solution and shown to yield satisfactory agreement. These results have important ramifications in accounting for deformation induced changes in hydraulic conductivity within fractured rock masses.*

## INTRODUCTION

Conductivity evaluations of fractured rock masses are of paramount importance in determining possible formation yields in the design of both resource exploitation and civil engineering projects. In such situations, it is important that the conductive behaviour of the mass may be characterized following perturbation of the groundwater regime and hence the appropriate changes in effective stress considered. The sensitivity of fissure flow to changes in fissure aperture has been widely reported [1, 2]. For laminar and turbulent flow, it may be shown that hydraulic discharge is proportional to the fissure aperture raised to the powers of 3 and 3/2, respectively. Changes in effective stress that promote mass displacements therefore have a profound effect on the fluid transmitting capability of individual fissures.

Displacements induced upon the rock mass discontinuities may be divided between pre-peak and post-peak modes. The former relate to the shear and normal stiffnesses of the discontinuities and have been reported to be intrinsically non-linear functions of applied stress [3, 4]. Although the pre-peak displacements are significant parameters in accounting for compatibility requirements in conventional modes of numerical analysis, they may be completely overshadowed by the magnitude of shear-dilational and tension related displacements, post-peak. These modes of failure may indeed be realized for unfavourably oriented planes of weakness adjacent to engineered rock structures.

The following text explores the possibility of characterizing the changes in the hydraulic conductivity of both matched and mis-matched rock fissures, of idealized form, under shear and normal displacements. Both sawtooth and sinusoidal forms are chosen and cases of non-tortuous and tortuous flow treated under laminar and turbulent flow conditions.

## ALTERNATE PROBLEM FORMULATIONS

Two distinct alternatives exist in determining the changes of hydraulic conductivity that will accompany a predetermined change in effective stress. The first of these represents a global approach whereby conductivity changes are measured directly on samples at a number of different stress levels. Conductivity changes may be measured within the laboratory [5, 6] under relatively well controlled boundary conditions or, they may be more tenuously deduced from field measurements [7]. In either case, the hydraulic conductivity at an elevated stress level for either an individual fissure or a portion of the formation may be deduced relative to the conduc-

* Department of Civil Engineering, University of Toronto, Toronto, Canada M5S 1A4. Currently, Department of Mineral Engineering, The Pennsylvania State University, University Park, PA 16802, U.S.A.
†Department of Civil Engineering, University of California, Berkeley, CA 94720, U.S.A.

tivity at a prescribed datum stress level. Shortcomings of this technique relate to both the complex nature of coupled stress level and conductivity testing, and the inability of empirical characterizations to account for the mixed mode deformations within the rock mass.

A second alternative in determining the stress dependent changes in conductivity involves the decomposition of the problem to the constitutive behaviour of the components constituting the system. The performance of individual components may be fully evaluated. In this manner, individual fissures may be tested to evaluate the hydraulic properties as a function of aperture distribution. Stress–deformation testing of fissures may be utilized to evaluate the change in fissure aperture distribution with stress level whereby both normal and shear deformational modes may be accommodated. Combination of these two results then completely defines the problem. The performance of a fractured rock mass may then be simulated numerically for any stress regime and arbitrary boundary conditions. This approach offers some saving in effort over the empirical or experimental approach if it is assumed that there is some unique relation between the aperture density distribution and the conductivity properties of a fissure. It is possible then to dispense with conductivity testing of individual fissures and the problem may be defined purely from stress deformation testing. The philosophy of separating fluid flow and stress–deformation characteristics is maintained in the following discussion.

## FISSURE HYDRAULICS

Relations between discharge rate and the environmental loading of potential gradient may be deduced from both analytical and empirical representations of the problem. The transmissivity term relating the discharge rate ($\mathbf{q}$) to the gradient ($\nabla\phi$) is linear only for laminar flow at low velocities. At high velocities and beyond the range of laminar flow, the transmissivity term is a non-linear function dependent on the potential gradient. These relations may be identified symbolically as

$$\{\mathbf{q}\} = [\mathbf{T}]\{\nabla\phi\} \quad \text{Linear flow} \tag{1}$$

$$\{\mathbf{q}\} = [\mathbf{T}(\nabla\phi)]\{\nabla\phi\} \quad \text{Non-linear flow} \tag{2}$$

where $\mathbf{T}$ is a transmissivity tensor. Characterization for the linear laminar and the non-linear turbulent regimes must be treated individually.

*Linear potential flow*

Analytical treatment of fissure flow is possible if the conduit is idealized to an analogy of flow between two parallel plates. This analogy is relatively consistent for saturated, laminar, incompressible flow where fluid transmission within the wall rock is negligible. If wall roughness is slight in relation to the mean fissure aperture, the parallel plate analogy yields the transmissivity of a single fissure as

$$T = \frac{g\,b^3}{12\nu} \tag{3}$$

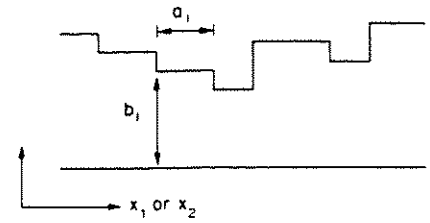


Fig. 1. Idealized geometric form for a single fracture within the plane (after Tsang and Witherspoon [10]).

where $T$ = transmissivity, $g$ = gravitational acceleration, b = mean fissure aperture and $\nu$ = fluid kinematic viscosity.

Numerous studies have addressed the characterization of rock fissures exhibiting significant wall roughness. The main concern within these studies has been to increase the fidelity of the relation between fissure aperture distribution and the corresponding fluid conductivity. Chronologically, the development has progressed from empirically derived conductivity coefficients [8], through thoughtful consideration and isolation of all contributing factors [9], to eventual attempts of analytical description [10–12]. This present study focuses on the last of these concepts in an attempt to extend characterization studies to dilatant fissures of idealized sinusoidal and sawtooth form.

*Analytical considerations*

The effect of the aperture distribution function on the resulting fluid transmission characteristics was studied analytically by Tsang and Witherspoon [10]. Considering the aperture to have a stepped profile as shown in Fig. 1, both longitudinal and transverse confined flow may be considered. For purely longitudinal flow across this profile, assuming no variation in aperture in the $x_1$-direction, the weighted average cubed fracture aperture (b) may be given by

$$\frac{\sum_j a_j b_j^3}{\sum_j a_j} = \langle b^3 \rangle_{x_{1,0}} \tag{4}$$

where $a_j$ and $b_j$ represent incremental step widths and apertures, respectively, as illustrated in Figs 1 and 2. The derivation of the equivalent fissure aperture of $\langle b^3 \rangle_{x_{1,0}}^{1/3}$ is directly analogous to that used in summing flow quantities for longitudinal flow in stratified deposits. Equa-

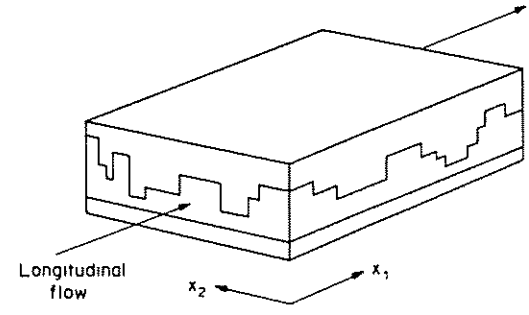


Fig. 2. Idealized geometric form for a single fracture in the transverse ($x_2$) or longitudinal ($x_1$) direction (after Tsang and Witherspoon [10]).

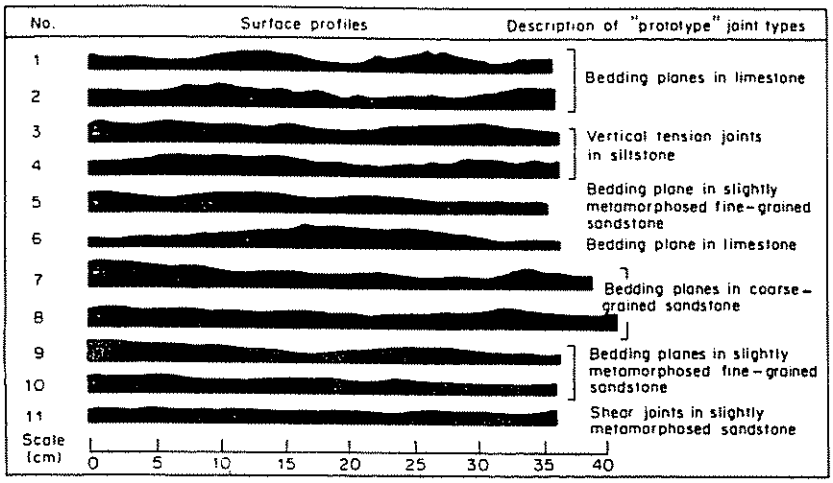


Fig. 3. Typical surface profiles from natural rock joints (after Bandis *et al.* [13]).

tion (4) is entirely sufficient if there is no variation in aperture in the longitudinal ($x_1$) direction. However, if this is not the case, the effect of this superimposed fissure aperture variation must be accounted for in the analysis. Summing the head drops along the mean direction of flow ($x_1$) yields

$$\frac{\Sigma a_j}{\Sigma b_j^2} = \left\langle \frac{a}{b^2} \right\rangle_{x_2=0}. \tag{5}$$

In a similar manner to (4), this expression is analogous to the case of transverse flow across a stratified deposit where the discrete system may be represented by a lumped parameter proportional to the gross hydraulic conductivity.

Combining (4) and (5) into an expression for flow within a rectangular block of fissure width W and length L, where flow tortuosity is neglected gives [10].

$$Q = \frac{W}{L}\frac{g}{12\nu}\langle b^3\rangle_{x_1}^{1/3}\frac{1}{\langle 1/b^2\rangle_{x_2}}[H(0) - H(x_1)] \tag{6}$$

where $Q$ represents discharge through the system and $[H(0) - H(x_1)]$ the head drop across the system.

If the variation in aperture distribution in the $x_1$- and $x_2$-directions are identical then flow may be considered proportional to $\langle b^3\rangle_{x_1}$. The assumption inherent within this treatment of the problem is that within the rectangular flow domain the streamlines and equipotentials remain respectively parallel and perpendicular to the longitudinal boundary of the flow domain. For tortuous flow, this assumption has been shown to be considerably in error. Former evaluations of this characterization scheme [10] had shown reasonable agreement with test data. Conflict in results arise because recent data reflect large spatial variations in fissure aperture within the samples studied whereas previous data had more homogeneous aperture distributions.

Characterization procedures utilizing the above methodology are extended for fissure configurations of assumed spatial distribution. An aperture density function fixed in space is used rather than a statistical distribution. The importance of using a known spatial distribution of aperture is evident if shear-dilation effects are to be examined in addition to normal closure. Additionally, the effects of tortuosity may be more fully evaluated and quantified.

Natural joints are observed as undulating surfaces in profile, typically of approximate sinusoidal or sawtooth form. Some examples of such features are shown in Fig. 3 for a variety of rock and joint types while Fig. 4 illustrates an attempted matching of a natural fracture by the idealized forms suggested above.

In the following sections, expressions are developed for flow within sinusoidal and sawtooth fractures subjected to shear deformation, dilation and normal closure.

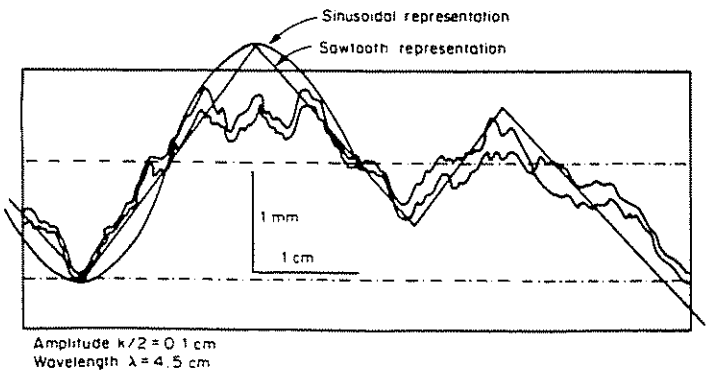


Fig. 4. Attempted matching of idealized sinusoidal and sawtooth forms on a real fissure profile (profile reported in Tsang [12]).

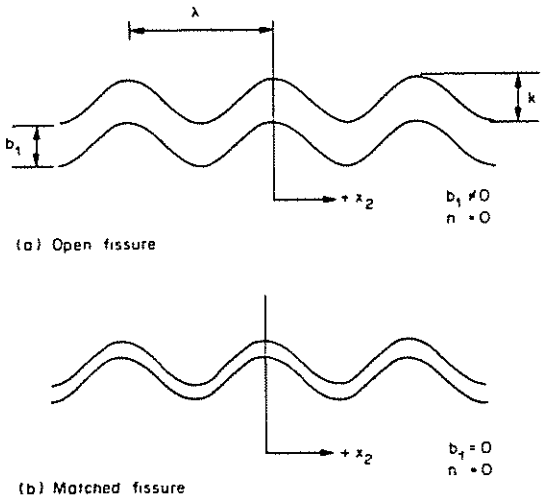


Fig. 5. Geometric representation of a mated sinusoidal fissure profile.

*Sinudoidal fissure*

The idealized geometric form of a matched sinusoidal fissure is shown in Fig. 5. The changes in aperture distribution resulting from shear and normal deformation are shown in Fig. 6. For flow transverse to this plane (out of the plane of the paper), with no variation in fissure aperture in the $x_1$-direction, the aperture (b) at any location is given by

$$\mathrm{b} = b_1 - k \sin\left(\frac{\pi n}{\lambda}\right) \sin\frac{2\pi x_2}{\lambda} \tag{7}$$

where $b_1$ = mean wall separation, $k$ = wall double amplitude and $n$ = shear offset.

For contacting fissure walls

$$b_1 = k \sin\frac{\pi n}{\lambda} \cdot 1. \tag{8}$$

Therefore

$$\mathrm{b} = k \sin\left(\frac{\pi n}{\lambda}\right)\left[1 - \sin\left(\frac{2\pi x_2}{\lambda}\right)\right] \tag{9}$$

gives the fissure aperture at any location along $x_2$. From this, $\langle \mathrm{b}^3 \rangle$ may be evaluated over any characteristic length, the smallest multiple of which must be a single

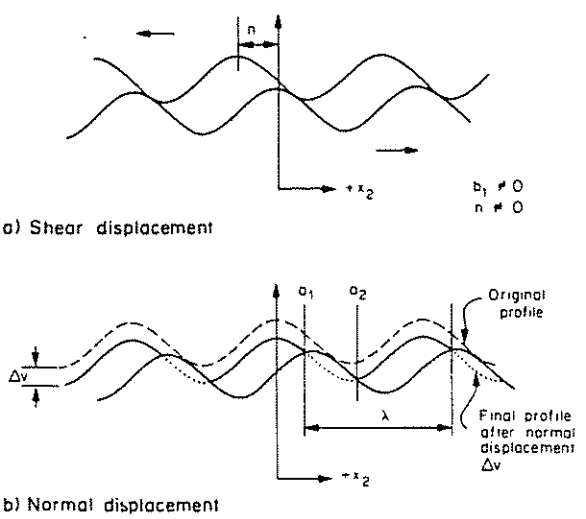


Fig. 6. Geometric representation of a mated sinusoidal fissure profile subject to relative displacement ($n$).

wavelength. Thus

$$\langle \mathrm{b}^3 \rangle_{x_{1,0}} = \frac{1}{\lambda}\int_0^{\lambda}\left[b_1 - k \sin\left(\frac{\pi n}{\lambda}\right) \sin\left(\frac{2\pi x_2}{\lambda}\right)\right]^3 \mathrm{d}x_2 \tag{10}$$

which for a non-mating fissure yields

$$\langle \mathrm{b}^3 \rangle_{x_{1,0}} = b_1^3 + \tfrac{3}{2} b_1 k^2 \sin^2\left(\frac{\pi n}{\lambda}\right) \tag{11}$$

and for contacting fissures, substitution of equation (8) into (11) gives

$$\langle \mathrm{b}^3 \rangle_{x_{1,0}} = \tfrac{5}{2} k^3 \sin^3\left(\frac{\pi n}{\lambda}\right). \tag{12}$$

Thus, the mean cubed aperture is defined for a sinusoidal fissure with either contacting or non-contacting faces for any arbitrary shear displacement. All that remains to complete the model is to define the change in mean cubed aperture that results from normal closure ($\Delta v$).

If it is assumed that under normal closure, the overlapping faces of the fissure may be discounted in the summation procedure it is possible to further define $\langle \mathrm{b}^3 \rangle$ according to Fig. 6.

The required term is equivalent to

$$\langle \mathrm{b}^3 \rangle = \frac{1}{\lambda}\left(\int_0^{\lambda} \mathrm{b}^3 \,\mathrm{d}x_2 - \int_{a_1}^{a_2} \mathrm{b}^3 \,\mathrm{d}x_2\right) \tag{13}$$

where b retains the same definition as given in equation (7). The limits of integration may similarly be defined as

$$a_1 = \frac{\lambda}{2\pi} \sin^{-1}\left[1 - \frac{\Delta v}{k \sin(\pi n/\lambda)}\right] \tag{14}$$

$$\sin a_2 = \sin(\pi - a_1) \tag{15}$$

Expansion of equation (13) yields

$$\frac{1}{\lambda}\int_0^{\lambda} \mathrm{b}^3 \,\mathrm{d}x_2 = (b_0 - \Delta v)^3 + \tfrac{3}{2}(b_0 - \Delta v) k^2 \sin^2\left(\frac{\pi n}{\lambda}\right) \tag{16}$$

$$\begin{aligned}\frac{1}{\lambda}\int_{a_1}^{a_2} \mathrm{b}^3 \,\mathrm{d}x_2 = \Bigg[&(b_0 - \Delta v)^3 x_2 + 3(b_0 - \Delta v)^2 k \sin\left(\frac{\pi n}{\lambda}\right) \\ &\times \frac{\lambda}{2\pi} \cos\left(\frac{2\pi x_2}{\lambda}\right) + 3(b_0 - \Delta v) k^2 \\ &\times \sin^2\frac{\pi n}{\lambda}\left(\frac{x_2}{2} - \frac{\lambda}{8\pi} \sin\left(\frac{4\pi x_2}{\lambda}\right)\right)\Bigg] \\ &+ k^3 \sin^3\left(\frac{\pi n}{\lambda}\right) \cdot \frac{\lambda}{2\pi} \cos\left(2\frac{\pi x_2}{\lambda}\right) \\ &\times \left[1 - \frac{1}{3}\cos^2\left(2\frac{\pi x_2}{\lambda}\right)\right]_{a_1}^{a_2} \frac{1}{\lambda}\end{aligned} \tag{17}$$

where $b_0$ is $b_1$ at the initial mating of the fissure walls as given in equation (8) and $\Delta v$ is the normal closure from this initial position. It is possible, therefore, to fully define the change in discharge for flow across this idealized sinusoidal fissure profile. Arbitrary shear and normal deformations may be specified.

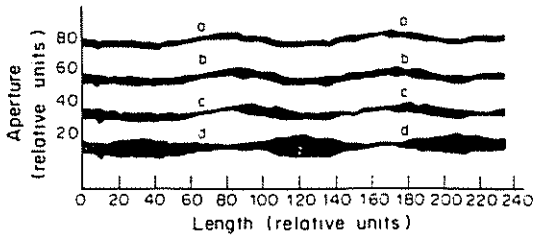


Fig. 7. Offset profiles of fissure surface number 1 subjected to increasing relative displacement $a$ through $d$ (after Tsang [11]).

An example illustrating the use of this technique will highlight the applicability of this procedure. From Fig. 3, fissure profile number 1 may be taken. Assuming that the fissure walls match, the assemblage may be subjected to initial shear deformations of different magnitudes as shown in Fig. 7. If a non-linear joint stiffness relation is applied to the problem [10] as idealized in Fig. 8, the normalized discharge as a function of normal stress may be evaluated. Results for discharge at the four different joint offsets of Fig. 7 are given in Fig. 9 under increasing normal load. It is encouraging that the results predict high transmissivity at low normal stress levels and drastic decreases in conductivity with increased ambient stress.

For transverse flow in a sinusoidal fissure, the theoretically derived expressions may be compared with the empirical results of Louis [8] given in Table 1. Longitudinal flow path lengths must be adjusted for the analytical expressions to yield physical equivalence. Equating the theoretical and empirical expressions and solving for the three dimensionless groups $b/k$, $n/\lambda$ and $b/\lambda$, the range over which both methods give identical results may be determined. A plot of this relation is given in Fig. 10 indicating the range of equivalence of two solution processes.

*Sawtooth fissure*

An alternative to a sine curve is a sawtooth fissure description as shown in Fig. 11. For transverse flow, similar expressions may be developed as for the sinusoidal case. For mating or non-mating sawtooth fractures

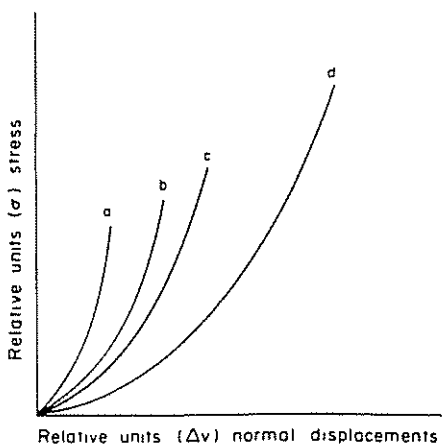


Fig. 8. Stress–fracture closure relation for fractures $a$ through $d$ in Fig. 7 (after Tsang [11]).

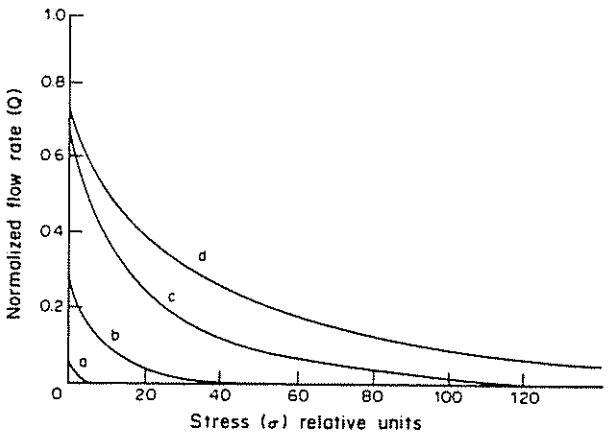


Fig. 9. Variation in normalized flow rate as a function of normal stress for mismatched sinusoidal fissures.

of geometry shown in the figure, the mean fissure aperture may be shown to be equivalent to

$$\langle b^m \rangle = \frac{\Delta u}{\lambda \Delta v (m+1)} [(\Delta v + b_1)^{m+1} - (b_1 - \Delta v)^{m+1}] + [(b_1 + \Delta v)^m + (b_1 - \Delta v)^m] \left( \frac{1}{2} - \frac{\Delta u}{\lambda} \right) \quad (18)$$

where $m$ = an arbitrary exponent and $\Delta u = n$ = shear offset.

The usefulness of defining the mean aperture as raised to any arbitrary power $m$ will be realized in dealing with the case of turbulent flow. Fluid transmission is then a

Table 1. Equivalent hydraulic conductivities

| Hydraulic zone | Hydraulic conductivity | Range of validity |
|---|---|---|
| 1 | $\frac{g b^2}{12\nu}$ | $0 < k/2b < 0.033$ |
| 4 | $\frac{g b^2}{12\nu(1 + 8.8(k/2b)^{1.2})}$ | $0.033 < k/2b < 0.5$ |

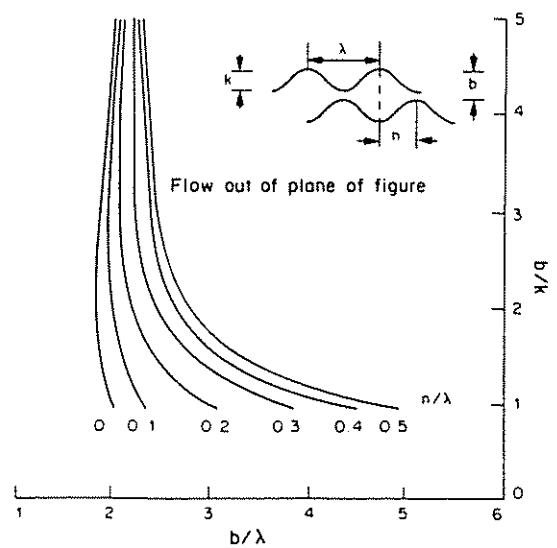


Fig. 10. Graphical representation of the dimensionless ratios $b/k$, $b/\lambda$ and $n/\lambda$ for which empirical results for fracture conductivity [8] are equivalent to the analytically derived conductivities. Laminar flow, sinusoidal fissure.

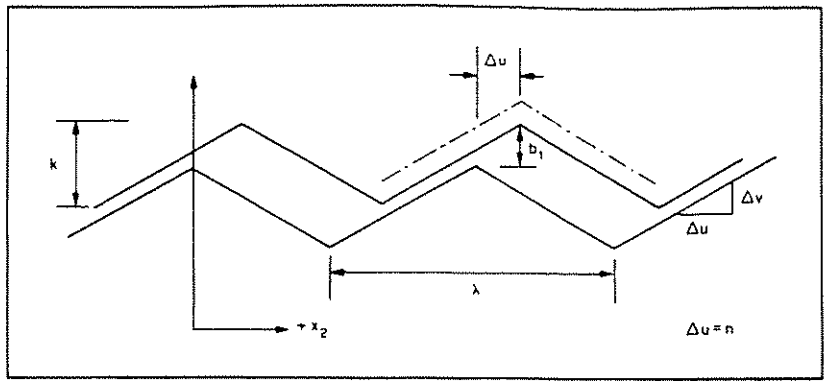


Fig. 11. Idealized geometric form for a sawtooth fissure profile.

function of mean aperture raised to the power 3/2. For the laminar case the exponent $m$ is 3 and $\langle b^3 \rangle$ may be evaluated from equation (18). For a mating fissure $b_1 = \Delta v$ and (18) reduces to

$$\langle b^3 \rangle = \frac{(2\Delta v)^3}{2}\left(1 - \frac{\Delta u}{\lambda}\right) \tag{19}$$

where

$$\Delta u = n \tag{20}$$

$$\Delta v = \frac{2nk}{\lambda}. \tag{21}$$

If the appropriate values of $\Delta u$ and $\Delta v$ are substituted into the sawtooth characterization equations, as given in (20) and (21), it is possible to compare the conductivities for the two idealized fissure forms. The ratios between sawtooth and sinusoidal conductivities are given in Fig. 12. The sawtooth idealization always returns a conductivity lower than that due to the sinusoidal representation. This effect is most pronounced for a contacting fissure and reduces as the aperture ($b_1$) increases relative to the undulation amplitude ($k$). Thus discharge for non-tortuous flow may be shown to be a function of the two dimensionless variables b/$k$ and $n/\lambda$. The change in discharge may be quantified merely in terms of the relative shear displacement $n/\lambda$ for a contacting fissure.

Figure 13 illustrates the increase in conductivity that results from dilation of a contacting fissure undergoing shear displacement. The sinusoidal fissure maintains a higher conductivity for all displacements consistent with Fig. 12.

*Tortuosity effects*

The previous study has considered longitudinal flow restricted within a transverse section invariant in profile. Tortuosity effects have been shown to have a profound effect on discharge [12]. Neglecting tortuosity may, therefore, lead to considerable error in conductivity characterization. These effects are minimized when the aperture density distribution is in the form of a spiked delta function and the fissure, by definition, faithfully represents the geometry of parallel plate flow. In this instance there is little variation in aperture magnitude in either of the two orthogonal in-plane co-ordinate directions. Streamlines and isopotentials form a near rectilinear grid and the conductivity may be approximated as proportional to $\langle b^3 \rangle$.

The aperture variation for a mating sinusoidal fissure may be represented in the two dimensional plane of a fissure as

$$b = \frac{k}{4}\sin\left(\frac{\pi n}{\lambda}\right)\left[2 - \sin\left(\frac{2\pi x_1}{\lambda}\right) - \sin\left(\frac{2\pi x_2}{\lambda}\right)\right] \tag{22}$$

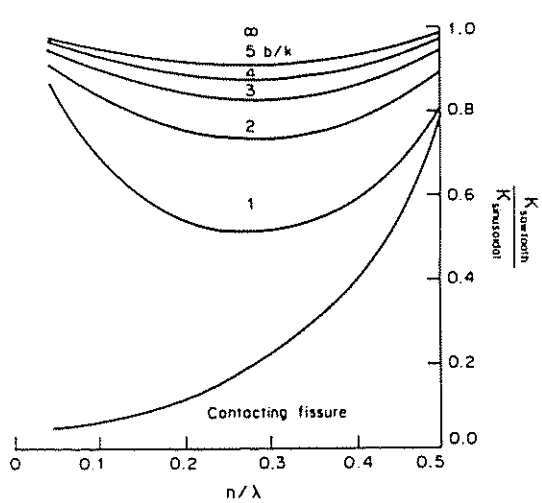


Fig. 12. Ratio of analytically derived conductivities for sawtooth and sinusoidal fissure profiles. Laminar flow.

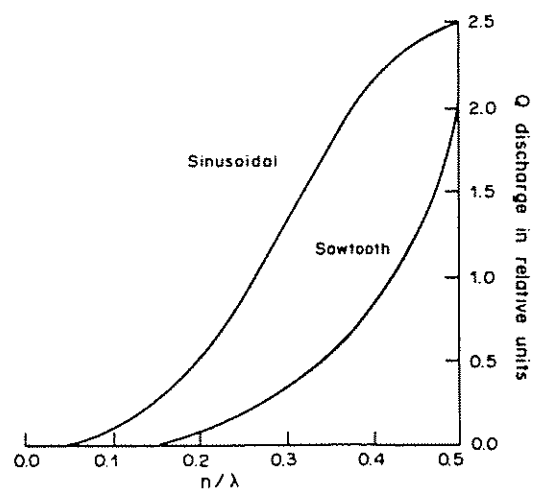


Fig. 13. Variation in normalized discharge for non-tortuous flow in sinusoidal and sawtooth fissures under a full range of shear displacements.

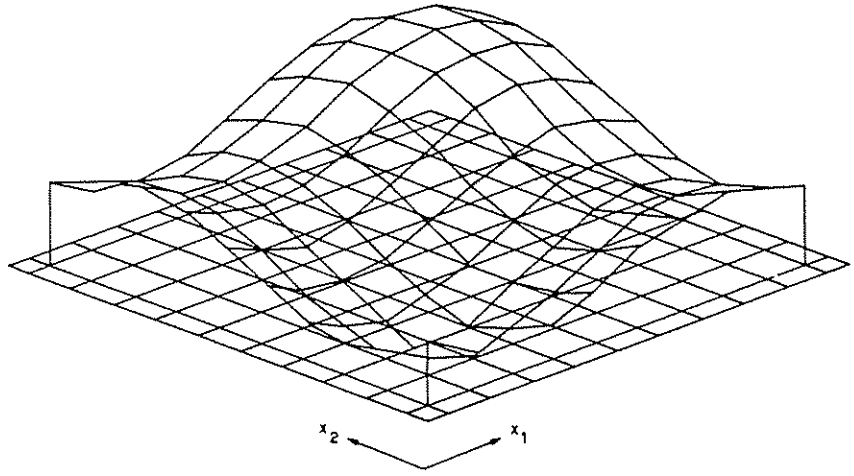


Fig. 14. Variation in fissure aperture for tortuous flow evaluations.

where the scaling factor on $k$ maintains the maximum and minimum fissure apertures equal to those for the one dimensional case as given in equation (9). The variation in fissure aperture in two dimensions is shown schematically in Fig. 14. The mean cubed aperture may be evaluated by integration in the two orthogonal coordinate direction as

$$\langle b^3\rangle_{x_1x_2} = \frac{1}{\lambda_1\lambda_2}\int_0^{\lambda_1}\int_0^{\lambda_2} b^3\,dx_1\,dx_2. \tag{23}$$

Asuming that the wavelengths $\lambda_1$ and $\lambda_2$ are identical for the most specific case yields

$$\langle b^3\rangle_{x_1x_2} = \tfrac{14}{64}k^3\sin^3\left(\frac{\pi n}{\lambda}\right). \tag{24}$$

This differs from the expression for non-tortuous flow as stated in equation (12)

$$\langle b^3\rangle_{x_1 0} = \tfrac{5}{2}k^3\sin^3\left(\frac{\pi n}{\lambda}\right). \tag{12}$$

Comparison of the two expressions indicates that consideration of a two dimensional variation in fissure aperture reduces the conductivity by over an order or magnitude. Although equation (24) is not rigorously correct (since it does not allow for non-rectilinear flow within the fissure) the result is qualitatively correct.

The validity of using the cubed fissure aperture averaged in two dimensions as an index of conductivity may be tested by numerical simulation. The plane of the fissure may be subdivided into a flow grid and appropriate conductivities assigned to each individual element. Solution by a steady state finite element code was utilized imposing a unit head drop on two opposite faces of a square region and a linear variation in head on the two remaining faces.

The results of this numerical simulation for a $10 \times 10$ grid of elements are shown in Fig. 15. Dimensionless discharge is shown as a function of relative shear displacement. The analytical and numerical results show favourable agreement considering that flow is markedly non-rectilinear. This facet of the analysis is illustrated in the contoured head distribution for the numerical testing in Fig. 16.

The tortuous nature of flow presents further problems in defining a discharge term in that inflow to the domain will occur on sides along which a linear variation in head is specified. This effect is shown by the plot of the fluid flux vectors in Fig. 17. However, for the

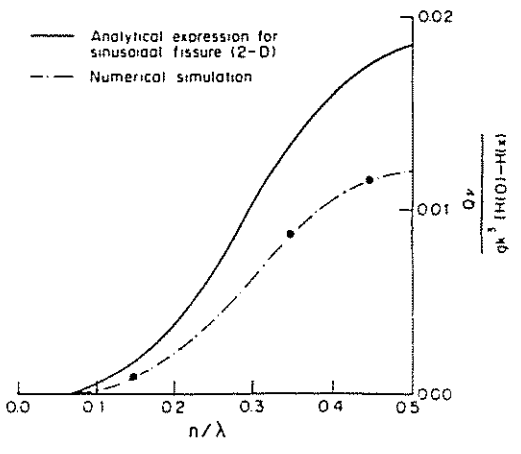


Fig. 15. Dimensionless discharge predicted from the analytical and numerical evaluations of tortuous flow in an idealized sinusoidal fissure.

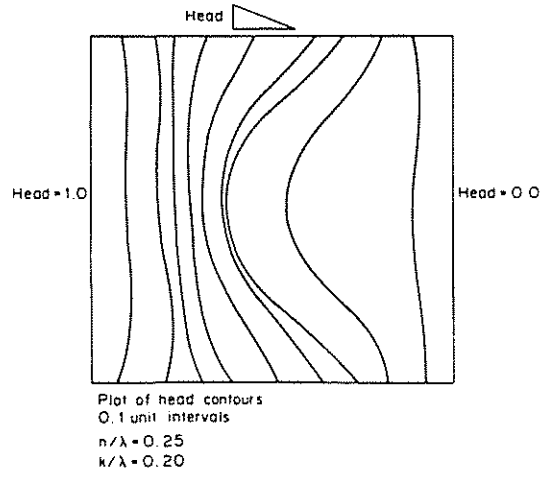


Fig. 16. Flow domain for the numerical simulations contoured to yield the variation in total head for tortuous flow.

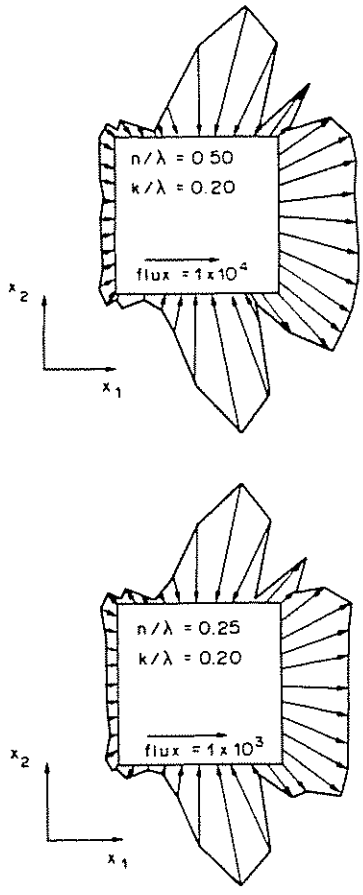


Fig. 17. Distribution of flux vectors for numerical simulation at two representative shear offsets.

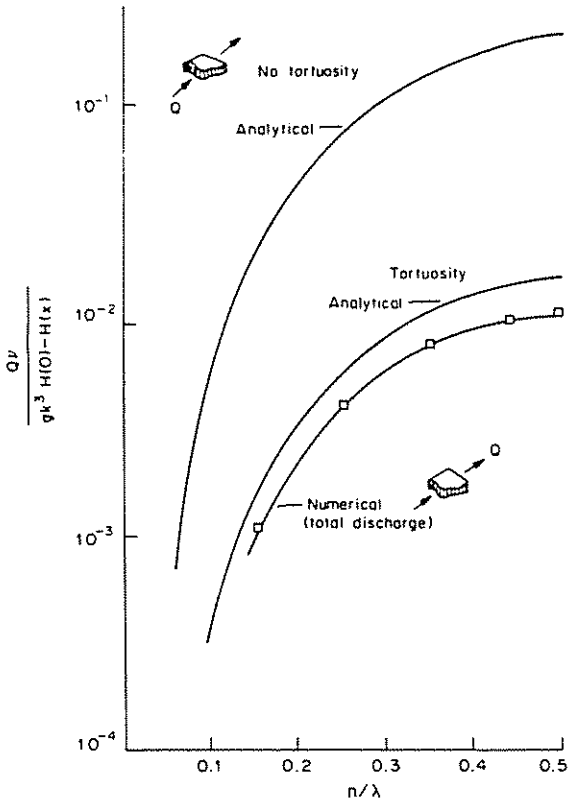


Fig. 18. Variation in dimensionless discharge as a function of relative shear displacement for both analytical and numerical conductivity evaluations.

purpose of this characterization, discharge is taken as total discharge from the flow domain.

A comparison between the numerical results and the analytical expressions for discharge is shown graphically in semi-log form in Fig. 18. The analytical expression for tortuous discharge through a two dimensional sinusoidal fissure overestimates discharge less than that for the non-tortuous case. It should be noted, however, that the expressions developed for non-tortuous flow are analytically correct. Their shortfall lies within the difficulty with which they may assimilate the true geometry of rock fissures. Comparison between the analytical and numerical simulations may be taken as conclusive in showing that tortuosity effects may be accommodated in some approximate manner within an analytical solution.

The concept may be extended for a contacting sawtooth fissure by following the same integration procedure for $\langle b^3 \rangle_{x_1 x_2}$. Conceptual problems in modelling this system arise in that the fissure variation of Fig. 11 in two dimensions leads to a sealed compartment with no entry or exit for fluid as illustrated in Fig. 19. This clearly negates the possibility of fluid transmission within the system. The sawtooth geometry is, however, considerably more convenient to handle for the case of integration schemes for turbulent flow in representing $\langle b^{3.2} \rangle_{x_1 x_2}$. Therefore, despite this limitation, $\langle b^m \rangle_{x_1 x_2}$ will be assumed a suitable index for tortuous flow within a sawtooth fissure. Integration of the aperture in two dimensions for Fig. 19 yields

$$\langle b^m \rangle_{x_1 x_2} = \frac{(2\Delta v)^m}{2} \left[ \frac{\Delta u}{\lambda_1} \left( \frac{2}{m+1} - 1 \right) + \frac{1}{2} \right]. \qquad (25)$$

which for equal wavelengths in the $x_1$- and $x_2$-directions and with $m$ equal to 3 reduces to

$$\langle b^3 \rangle_{x_1 x_2} = \frac{(2\Delta v)^3}{4} \left( 1 - \frac{\Delta u}{\lambda} \right). \qquad (26)$$

For linear, laminar flow within an irregular fissure, it appears that an averaged fissure aperture provides the only presently tractable method of flow characterization. The variation in fissure aperture may be described by some spatial function as attempted in this work. The advantage of having knowledge of the spatial variation is that the effect of dilation may be evaluated. Dilation

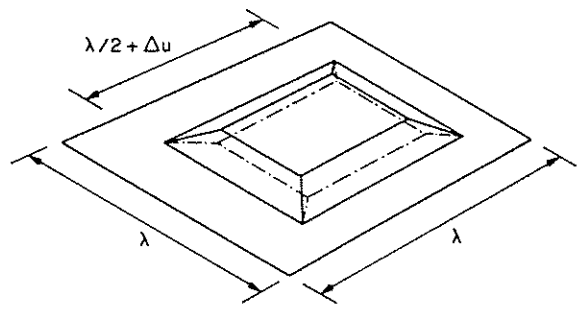


Fig. 19. Geometric description of a sawtooth fissure in three dimensional form.

is clearly important in situations where shear deformation may result from mechanical or hydraulic loading of individual fissures.

*Non-linear potential flow*

The non-linearity inferred in this context is that discharge rate is no longer directly proportional to hydraulic gradient. The transmissivity tensor for the fissure is consequently a non-linear function of gradient and may be expressed symbolically as

$$\{\mathbf{q}\} = [\mathbf{T}(\nabla\phi)]\{\nabla\phi\}. \tag{2}$$

The non-linearity results from the mixed interference of inertial and kinetic effects, both of which may be substantial for high velocity flow.

*Inertial effects.* Inertial effects are manifest where spatial accelerations within the flow domain are apparent. Accelerations result from flow convergence or divergence and may be envisaged to occur adjacent to well bores or in fissures tapering in the direction of flow. This effect is not exhibited in plane, non-tapering flow situations.

The importance of inertial effects may be quantified for any given flow domain by recourse to an inertial factor [9]. This factor essentially represents the ratio of inertial to frictional loss within the system and may be stated as

$$\eta = \frac{|v\,\partial v/\partial x_1|}{|-g\,\partial\phi/\partial x_1|} \tag{27}$$

where $v$ and $\partial v/\partial x_1$ are respectively the flow velocity and gradient of velocity and $\partial\phi/\partial x_1$ represents the total head gradient. For laminar flow, inertial effects may be considered as only of significance for values of $\eta$ greater than 0.5. Thus, if values of $\eta$ may be maintained below this threshold, inertial effects may be neglected.

*Kinetic effects.* Kinetic effects result from head losses at increased flow velocities being dependent on velocity head in addition to the potential head. For low velocity flows, the kinetic head loss is negligible in comparison to potential head loss and may be neglected. However, for flow in fissure systems, kinetic losses may account for a significant portion of the total losses.

In addition to kinetic losses, turbulent flow may be manifest at increased flow velocities. The onset of turbulence may be indexed by recourse to the critical Reynolds number. For flow in rock fissures, the Reynolds number may be defined as

$$\mathrm{R_e} = \frac{v\,2\mathrm{b}}{\nu} \tag{28}$$

where $v$ = velocity, b = mean fissure aperture and $\nu$ = fluid kinematic viscosity. For rock fissures, the critical Reynolds number commonly lies between 100 and 2300, increasing from the lower datum with decreasing joint wall relative roughness.

In conductivity testing of fissures it is not possible to separate the effects of kinetic and turbulent loss explicitly since both effects may be manifest simultaneously and to varying degrees. Non-linear criteria may be identified to describe this phenomenon.

Two flow laws have been proposed to relate flow velocity to hydraulic gradient in a non-linear manner. These relations are summarized in recent literature [14, 15]. The first of these is the Forchheimer law using a polynominal expression to describe the velocity dependant gradient ($\nabla\phi$) as

$$\nabla\phi = av + bv^2 \tag{29}$$

where $a$ and $b$ are constants and $v$ represents the flow velocity in the direction of maximum gradient. Constants $a$ and $b$ are determined experimentally and are properties of the fluid and transmitting medium. The constants are only applicable over a given range of flow velocities, outside which, revised parameters must be substituted. For low velocity flows, constant $a$ is much larger than $b$ and the expression reduces to the normal Darcy law. The validity of this relation has been inferred from both experimental results and from manipulation of the Navier–Stokes equations.

A second relation between hydraulic gradient and flow velocity is the Missbach law in the form of a power function

$$\nabla\phi = cv^m \tag{30}$$

where $c$ is a proportionality constant and $m$ is an exponent ranging between 1 and 2. The magnitudes of both $c$ and $m$ vary with flow velocity although may be sensibly constant over a given range. The validity of the law has been confirmed for fissure flow in simulated rock fractures by Louis [8]. These flow laws enable the conductance of a fissure of known geometry to be determined uniquely as a function of flow velocity. The Missbach law in equation (30) may be rewritten as

$$v = -K\nabla\phi^{\alpha} \tag{31}$$

where $K$ represents the hydraulic conductivity of the fissure and $\alpha$ is equal to unity for laminar flow and 1/2 for turbulent flow in a rough walled fracture. Suitable values of $K$ and the range of validity of the laminar regime are obtained from the work of Louis [8]. Fissure conductivity is a function of aperture and fissure wall relative roughness ($k$/2b) with a critical Reynolds num-

Table 2. Equivalent hydraulic conductivities (from Louis [8]) NB. $D_h = 2\mathrm{b}$.

| Hydraulic zone | Hydraulic conductivity (L/T) | Exponent ($\alpha$) |
|---|---|---|
| 1 | $\frac{g\mathrm{b}^2}{12\nu}$ | 1.0 |
| 2 | $\frac{1}{\mathrm{b}}\left[\frac{g}{0.079}\left(\frac{2}{\nu}\right)^{1/4}\mathrm{b}^{1}\right]^{4/7}$ | 4/7 |
| 3 | $4g^{1/2}\log\left[\frac{3.7}{k/D_h}\right]\mathrm{b}^{1/2}$ | 0.5 |
| 4 | $\frac{g\mathrm{b}^2}{12\nu(1+8.8(D_h)^{3/2})}$ | 1.0 |
| 5 | $4g^{1/2}\log\left[\frac{1.9}{(k/D_h)}\right]\mathrm{b}^{1/2}$ | 0.5 |

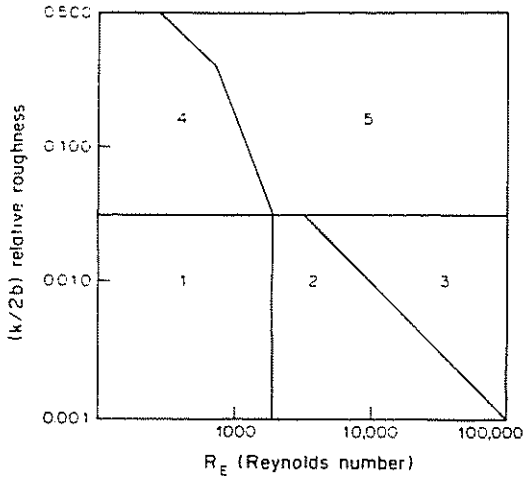


Fig. 20. Hydraulic flow regions (after Louis [8]).

ber being ascribed for any given fissure relative roughness to delineate the transition from laminar to turbulent flow. The empirical results for the constants $K$ and $\alpha$ are shown in Table 2. The range of validity of these parameters as a function of the dimensionless parameters of relative roughness ($k/2b$) and Reynolds number are shown in Fig. 20. The form of non-linear conductivity is shown in Fig. 21 as a function of gradient beyond a threshold gradient for a number of representative fissure apertures.

The two phases of flow in the laminar and turbulent regime give

$$\text{Laminar} \qquad v = K_L \nabla\phi \qquad \nabla\phi = \frac{v}{K_L} \tag{32}$$

$$\text{Turbulent} \qquad v = K_T(\nabla\phi)^{1/2} \qquad \nabla\phi = \frac{v^2}{K_T^2}. \tag{33}$$

The Missbach relation implies that flow is linear until the onset of turbulence. Beyond this threshold, the effect of kinetic head in contributing to total head loss is considered. The implication of this is that head loss due to velocity effects is only considered beyond the turbulent threshold rather than as a continuous function of velocity as in the Forchheimer relation. The Missbach relationship is analogous to the Forchheimer relation where the coefficients $a$ and $b$ may be substituted as

$$\text{Laminar} \qquad a = \frac{1}{K_L} \qquad b = 0 \tag{34}$$

$$\text{Turbulent} \qquad a = 0 \qquad b = \frac{1}{K_T^2}. \tag{35}$$

Throughout this work, the Missbach flow law is used to characterize the full flow regime. This is the form in which the only authoritative experimental data on the subject are reported.

Methods identical to those outlined previously may be used to characterize equivalent fissure apertures for flow under turbulent conditions. For non-tortuous flow the discharge may be represented as

$$q = \frac{W}{L} \cdot \langle b^{3/2} \rangle_{x_1} [H(0) - H(x)] \cdot d \tag{36}$$

where W = flow domain width, L = flow domain length, $d$ is an experimentally determined coefficient and $q$ = discharge rate. Thus, the average fissure aperture should be evaluated to the power 3/2. The sawtooth representation of fissure geometry is most convenient and yields for the case of a contacting fissure

$$\langle b^{3/2} \rangle_{x_1} = (2\Delta v)^{3/2} \left( \frac{1}{2} - \frac{\Delta u}{5\lambda} \right). \tag{37}$$

As was determined previously however, the two dimensional realization of such a fissure may be more appropriate in determining the true flow characteristics. In this instance equation (25) yields

$$\langle b^{3/2} \rangle_{x_1 x_2} = \frac{(2\Delta v)^{3/2}}{2} \left( \frac{1}{2} - \frac{\Delta u}{5\lambda} \right). \tag{38}$$

As mentioned previously, the geometry of a trapezoidal flow compartment is difficult to justify as entry into the fissure is sealed on all four sides as shown in Fig. 19. No other tractable solution is, however, currently feasible. Fissure apertures weighted in this manner may be used to determine conductivity changes resulting from shear and normal deformations.

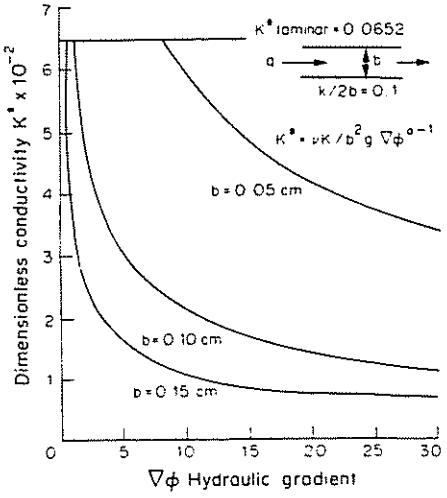


Fig. 21. Variation in dimensionless conductivity with hydraulic gradient.

## DISCUSSION

The accuracy of the conductivity predictions made from the procedures outlined above may only be viewed in the light of the adequacies of the respective fissure idealizations. Clearly, the form of real rock fisures may only be crudely approximated by sinusoidal or sawtooth forms. Logical extension of the work would involve spatial discretization of real rock profiles accompanied by numerical summation to evaluate the parameters $\langle b^3 \rangle$ or $\langle b^{3/2} \rangle$ as appropriate. In this approach, however, the analytical simplicity is lost and trends in overall behaviour may not readily be identified. From this viewpoint, the concepts presented herein are believed most useful.

For non-tortuous flow, the analytical results are exact since all physical and analytical assumptions are compatible. A physical analogy to the geometry envisaged for non-tortuous flow might be flow along the crest axes of ripple marks and their corresponding casts in sedimentary deposits. With shear occurring transverse to the structures, the accompanying dilation greatly enhances the longitudinal hydraulic conductivity up to a maximum for a contacting fissure. Both sinusoidal and sawtooth forms of fissure roughness may be accommodated with equal ease. Choice of either form would rest with the adequacy to which either idealization represents the true situation. It is noted that conductivities derived from a sawtooth idealization are always lower than those for sunusoidal surfaces at corresponding shear and normal offsets. The conductivities of the two forms only approach equality in the limit as the normal separation is increased (Fig. 12).

The analytically derived conductivities and those evaluated from empirical results [8] may be compared only if due allowance is made for roughness in two orthogonal directions. In the comparisons, it is assumed that there is an undulation in fissure profile measured along the length of flow and that this undulation is identical to that in the transverse direction. However, flow is maintained to be non-tortuous requiring that there is no change in aperture in the longitudinal ($x_1$) direction. Consequently, a constant aperture is superimposed upon the undulation form of the fissure profile. Based on these assumptions, the empirical and analytical results are shown to be equivalent for single values of the ratio of mean fissure aperture to fissure wavelength ($b/\lambda$). Such comparisons allow some conclusions to be drawn as to the applicability of the analytical characterization scheme although the empirical results were only reported, in their original form, for non-contacting fissure walls.

The importance of considering tortuosity in flow cannot be underestimated in the characterization process. In this treatment, a representative sinusoidal variation in fissure aperture in two dimensions has been used to evaluate the effectiveness of the summed $\langle b^3 \rangle$ technique for tortuous flow. Although, in the example considered, flow may be recognized to be tortuous, the degree of tortuosity is low with the simulated fissure profile containing a single point of mating. From recognition of this factor, the analogous physical situation would be a fissure under low ambient normal stress. The procedure is, however, not limited to this low ambient stress state and may accommodate any arbitrary magnitude of closure.

Although for tortuous flow, the flow path pattern is markedly non-rectilinear, excellent agreement is maintained between the analytical characterization and the numerical simulation. Indeed, the level of agreement is encouraging. One of the necessary characteristics of tortuous flow is that a gradient applied in one direction may induce flow in a direction non-parallel to the orientation of the maximum global gradient. In this manner therefore, account must be taken of the fact that the throughput of the system is not isolated purely to the inflow and outflow faces as illustrated in Fig. 17. In this work, the total throughflow has been used as the characteristic discharge quantity in the evaluations.

Where flow may be expected to exit the laminar regime and become turbulent, the appropriate aperture to be used in characterization studies is the mean fissure aperture to the power 3/2. No suitable flow analogy is available for this case of turbulent flow with the mean aperture to the power 3/2 requiring to be accommodated in the empirical relations.

## CONCLUSION

From the previous text it is evident that characterization of the form presented herein can constitute a valuable procedure in evaluating post-peak shear strength change in hydraulic conductivity. The analytical treatment for the case of non-tortuous flow is exact, although physical situations directly analogous to the geometry are somewhat limited. Conversely, the analytical treatment for tortuous flow is approximate in that the non-rectilinearity of flow may not be accommodated in closed form. The geometry is, however, more amenable to physical description and as such more representative of real rock fissure profiles.

*Acknowledgements*—The authors gratefully acknowledge support for this work obtained from American Electric Power Service Corp. and the Directors Fund of the Lawrence Berkeley Laboratory.

*Received* 24 *April* 1985.

## REFERENCES

1. Snow D. T. A parallel plate model of fractured permeable media. Ph.D. thesis, Univ. of California, Berkeley (1965).
2. Maini Y. N. T. *In situ* parameters in jointed rock—their measurement and interpretation. Ph.D. thesis, Imperial College of Science and Technology, London Univ. (1971).
3. Goodman R. E. The mechanical properties of joints. *Proc. 3rd Int. Congr. on Rock Mechanics*, Montreux (1979).
4. Goodman R. E. *Methods of Geological Engineering in Discontinuous Rocks*. West, St. Paul (1975).
5. Ohnishi Y. Laboratory measurement of induced water pressure in jointed rocks. Ph.D. thesis, Univ. of California, Berkeley (1973).
6. Gale J. E. Effects of fracture type (induced versus natural) on the stress-fracture closure-fracture permeability relationships. *Proc. 23rd U.S. Symp. on Rock Mechanics*, Univ. of California, Berkeley (1982).
7. Louis C. Rock hydraulics in rock mechanics, pp. 299–387. A course held by CISM, Udine. Springer Verlag, Vienna (1974).
8. Louis C. A study of groundwater flow in jointed rock and its influence on the stability of rock masses. Imperial College Rock Mechanics Research Rept No. 10, September (1969).
9. Iwai K. Fundamental studies of flow through a single fracture. Ph.D. thesis, Univ. of California, Berkeley (1976).
10. Tsang Y. W. and Witherspoon P. A. Hydromechanical behaviour of a deformable rock fracture due to normal stress. *J. Geophys. Res.* **86(B10)**, 9287–9298 (1981).
11. Tsang Y. W. and Witherspoon P. A. The dependence of fracture mechanical and fluid properties on fracture roughness and sample size. *J. Geophys. Res.* **88(B3)**, 2359–2366 (1983).
12. Tsang Y. W. The effect of tortuosity on fluid flow through a single fracture. *J. Geophys. Res.* (In press).
13. Bandis S., Lumsden A. C. and Barton N. R. Experimental studies of scale effects on the shear behavior of rock joints. *Int. J. Rock Mech. Min. Sci. & Geomech. Abstr.* **18**, 1–21 (1981).
14. Volker R. E. Nonlinear flow through porous medis by finite elements. *J. Hydraul. Div. Am. Soc. av. Engrs* **HY6**, 2093–2114 (November, 1969).
15. Trollope D. H., Stark K. P. and Volker R. E. Complex flow through porous media. *Aust Geomech. J.* **G1**, No. 1 (1971).